Materiales de Construcción 75 (359)
July-September 2025, e384
ISSN-L: 0465-2746
https://doi.org/10.3989/mc.2025.383324

Utilization of thermal-activated copper tailings as a partial substitute for cement: a promising approach

L. Wang[a], H. Fang[a] ✉, P. Chen[a,b], Z. Zong[a], P. Qian[a], X. Wang[a]

a. School of Civil Engineering and Architecture, Anhui University of Science and Technology, (Anhui, China)
b. State Key Laboratory of Mining Response and Disaster and Control in Deep Coal Mines, Anhui University of Science and Technology, (Anhui, China)
✉: 13731945032@163.com

Received 4 May 2024
Accepted 27 January 2025
Available on line 11 March 2026

ABSTRACT: This study proposed thermal activation to activate copper tailings and investigated the effects of the temperature of thermal activation on the hydration properties, pore structure, and compressive strength of thermally activated CT (TCT) pastes. The results indicate that thermal activation slightly refines the particle size of CT and induces the decomposition of $CaCO_3$, leading to the formation of highly reactive CaO. Compared to raw CT, the addition of calcined CT in the pastes resulted in a greater quantity of early hydration products, with increases of 0.34%—5.6% in C-S-H and ettringite, and approximately 0.9%—15.7% in $Ca(OH)_2$. These changes facilitated a reduction in paste porosity, resulting in a more densified structure. Consequently, the compressive strength of TCT pastes increased by 6.8%—20.6% at 3d, by 5%—16.9% at 7d, and by 1.2%—13.5% at 28d. Therefore, the proposed thermal activation CT can be a promising cement substitution.

KEY WORDS: Copper tailings; Thermal activation; CaO; Hydration; Compressive strength.

Citation/Citar como: Wang L, Fang H, Chen P, Zong Z, Qian P, Wang X. 2025. Utilization of thermal-activated copper tailings as a partial substitute for cement: a promising approach. Mater. Construcc. 75(359):e384. https://doi.org/10.3989/mc.2025.383324

RESUMEN: *Utilización de residuos de cobre activados térmicamente como sustituto parcial del cemento: un enfoque prometedor.* Este estudio propone la activación térmica de residuos de cobre y evalúa su efecto en las propiedades de hidratación, la estructura de poros y la resistencia a la compresión de pastas con residuos de cobre activados térmicamente (TCT). Los resultados indican que la activación térmica reduce el tamaño de las partículas de CT e induce la descomposición de $CaCO_3$, generando CaO altamente reactivo. La adición de CT calcinado aumenta los productos de hidratación temprana, con incrementos de 0.34% a 5.6% en C-S-H y etringita, y de 0.9% a 15.7% en $Ca(OH)_2$. Estos cambios reducen la porosidad de la pasta, resultando en una estructura más densificada. La resistencia a la compresión de las pastas de TCT aumenta entre 6.8% y 20.6% a los 3 días, y entre 1.2% y 16.9% a los 28 días. Así, el CT activado térmicamente puede ser una alternativa prometedora al cemento.

PALABRAS CLAVE: Residuos de cobre; Activación térmica; CaO; Hidratación; Resistencia a la compresión.

1. INTRODUCTION

Copper tailings (CT) are mineral wastes produced during the copper smelting process, primarily composed of quartz, sodium feldspar, calcite, and dolomite (1). The growing global demand for copper products has led to a significant increase in CT production as an industrial by-product (2, 3). Reports indicate that approximately 3.2 billion tons of CT are generated globally each year (4). Despite previous attempts to use CT for purposes of mining backfill (5-7) or roadbed material (8), the practical utilization of CT has been restricted due to factors like fine size, low reactivity, and heavy metal pollution of CT (9-11). Consequently, large amounts of CT are still directly dumped in tailings ponds, requiring huge investments in both construction and maintenance, while the possible dam break or tailings leakage risk also hazards ecological safety (12-15). Based on these challenges, it is important to develop effective methods for the utilization of CT.

Studies (13, 16, 17) have highlighted the high silica content and similar particle size of CT to that of cement particles and did not require additional grinding. Therefore, researchers suggest using CT as a part of concrete materials to utilize this mineral waste in large quantities, e.g., the substitution of partial cement (18-20). For instance, Moura et al. (21) confirmed the compatibility of using CT as a partial replacement for cement in concrete. The results have shown a 2.3% increase in compressive strength with 20% CT, along with an obvious 24.1% reduction in capillary absorption, and up to 35.7% in carbonation depth. Onuaguluchi et al. (22) reported an increment of acid resistance by 21% and chlorine resistance by 23% of mortars with 10% CT, without reducing the compressive strength. Additionally, the use of CT in concrete was also found to immobilize heavy metal elements, as reported by Ghazi et al. (2). These studies present viable perspectives on preparing concrete with CT. Nevertheless, the low reactivity of CT makes it an unqualified cementitious material to provide sufficient bonding effect for the prepared concrete (23, 24). The resulting concrete normally suffers from decreased compressive strength with the excessive addition of CT. For instance, Jenni et al. (25) investigated the influence of the substitution ratio of CT to cement in mortar preparation. It was found that the addition of 25% CT caused a significant reduction of 24% in the 90d compressive strength of mortars. When further increasing the amount of CT to 75—90%, the 90d compressive strength is even reduced by more than 80%. Therefore, it is necessary to activate it and further study the activation of the activity of the tailings.

Numerous studies have reported on the activation of tailings for the production of cementitious materials, including mechanical, thermal, and chemical activation methods (12, 26-28). Thermal activation of tailings generally occurs through two main mechanisms: (a) due to the different volatilization temperatures of mineral components, thermal activation can remove impurities in the mineral through volatilization (29), (b) changing the mineral crystal phase through heat treatment (30). Both mechanisms enhance the disorder or exposure of active ions or groups, promoting their participation in cementitious reactions (31). For example, Xiao and Pang (32) demonstrated that high-temperature calcination can remove volatile impurities from diatomite, improve porosity and surface structure, and thus enhance its pozzolanic activity. Fernandez et al. (31) found that kaolinite has significant thermal activation potential, where calcination induced dehydroxylation, producing reactive metakaolin, which improved the mechanical properties of cement-based mixtures. Similarly, Baki et al. (33) optimized the pozzolanic reactivity of minerals by calcination, transforming calcite into amorphous lime, which significantly enhanced the pozzolanic response of clays and marl. Given the high carbonate content in CT, it possesses substantial thermal activation potential. Therefore, in this study, we employed thermal activation of CT to enhance its reactivity and make it suitable as a supplementary cementitious material in cement systems.

To this end, this paper will calcine CT using different temperatures (400—900 ℃) to examine the influence of activating temperature on the properties of CT. Moreover, the influence of the produced thermal-activated CT (TCT) on the setting time, fluidity, hydration products, compressive strength, pore structure, and microstructure of CT are studied. The contributions of this paper are to reveal the effects of thermally activated CT on the cement hydration process and provide a valuable reference on the thermal activation of other tailings.

2. MATERIALS AND METHODOLOGY

2.1. Raw materials

Portland cement (P. O. 42.5) was purchased from Anhui Conch Cement Co., Ltd. CT with an apparent density of 2.8 g/cm^3 was provided by Chuzhou Tongxin Mining Co., LTD. The particle size shown by the raw CT is similar to that of the cement shown in Figure 1a, while its mineralogy is mainly composed of SiO_2, $CaCO_3$, and mayenite. Table 1 shows the chemical compositions of raw CT by X-ray fluorescence. The raw CT contained the highest amount of CaO (37.46%) as the main component, followed by SiO_2 (32.53%) and Fe_2O_3 (20.58%). In this study, CT is used as a supplementary cementitious material. Before the experiment, the raw CT was calcined in a Muffle furnace for 2h at 400 ℃,500 ℃,600 ℃,700 ℃,800 ℃, and 900 ℃, respectively. Tap water was used as mixing water.

Table 1. Chemical composition of the used cement and raw CT /%.

	SiO_2	CaO	Fe_2O_3	Al_2O_3	MgO	SO_3	K_2O	TiO_2	CuO	LOI	Others
Cement	21.07	60.22	3.65	8.82	1.36	2.81	/	/	/	1.34	2.07
CT	32.53	37.46	20.58	4.67	2.34	0.21	0.63	0.25	0.06	5.5	1.27

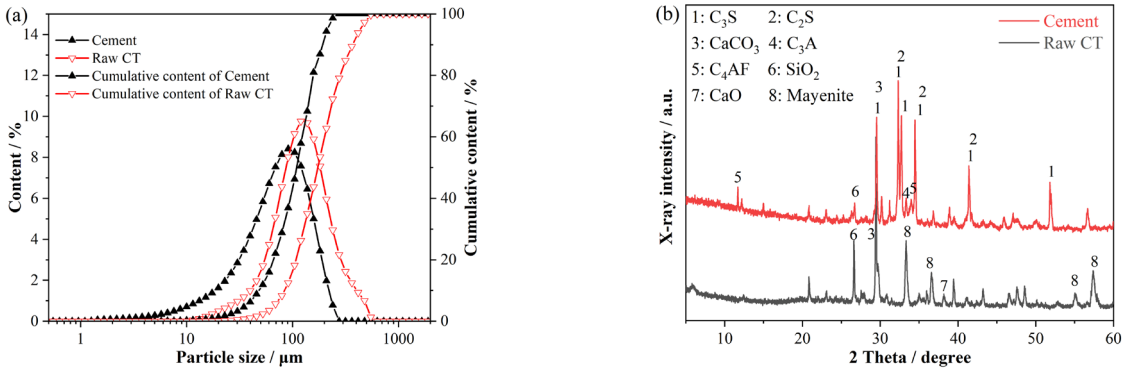

Figure 1. The particle size (a) and the XRD patterns (b) of cement and raw CT.

2.2. Mixtures preparation

Preparing seven mixtures with a water-cement ratio of 0.35 and 10% CT substitute for cement; the mixture proportion of pastes is shown in Table 2. The cement and CT were mixed thoroughly for 2 minutes and then added water to continuously mixed for an additional 3 minutes. The marked CT0 represents the mixture that uses raw CT, while TCT4—9 indicates the use of CTs that calcined at 400—900 °C, respectively, with a 100 °C span.

Table 2. Mix proportion of CT pastes / kg/m³.

Mixture	Cement	CTs	Water	Activation temperature
CT0	2700	300	1050	/
TCT4	2700	300	1050	400 °C
TCT5	2700	300	1050	500 °C
TCT6	2700	300	1050	600 °C
TCT7	2700	300	1050	700 °C
TCT8	2700	300	1050	800 °C
TCT9	2700	300	1050	900 °C

2.3. Analysis methods

2.3.1. Physical characterization

A Mastersizer 2000 laser diffractometer was used to measure the particle size distributions of CT. Using ethyl alcohol (refractive index 1.36) as a dispersing agent, while the refractive indices of the solid materials in CT were also considered as calcium carbonate (refractive index 1.49) and silica (refractive index 1.52). The particle sizes of CT were measured by stirring 5 times at 2000 rpm for 12s, obtaining an averaging of results. A Rigaku Smartlab X-ray diffractometer (XRD) was applied to detect the composition of mineral phases of CT, with the scanning speed range set at 5°/min and the measurement angle was 5° to 60°. Before the test, all the specimens were vacuum drying for 2h.

2.3.2. Setting time

The impact of thermal-activated CT on the setting times of the pastes was examined by the Vicat needle test in accordance with ASTM C191 (34).

2.3.3. Flowability

An STNLD-3 fluidity tester was applied to test the fluidity of the mortars according to ASTM C1437 (35). Fresh mortars are placed in the truncated conical mold and vibrated 25 times. The average diameter of the sample unfolded in both orthogonal directions was recorded.

2.3.4. Hydration products analysis

Collecting samples from the produced pastes after curing 3d and 28d, and after that, soaked in isopropanol alcohol for a minimum of 7d to stop further cement hydration. The collected samples were then vacuum-dried for 24h and ground to fine powder that was less than 75μm. A Rigaku Smartlab X-ray diffractometer was used to detect the characterized crystalline phases of CT pastes, with the scanning speed range and measurement angle were 5°/min and from 5° to 60°, respectively.

Thermogravimetric-differential thermal (TG-DTG) analysis was performed using a TA Q5000IR thermogravimetric analyzer to further quantify the hydration products. Before testing, the specimens were ground to fine powders that were less than 75μm with about 25mg per sample. After that, they were subjected to a heating profile from 30 °C to 800 °C in a nitrogen (N_2) atmosphere at a rate of 20 °C/min.

2.3.5. Pore structure by nuclear magnetic resonance (NMR)

The pore structure analysis of 28d CT pastes was conducted using a MesoMR23–060 V-1 Newman NMR instrument. The cylindrical sample with a diameter and height of 50 mm was prepared following the process of mixture preparation. Before testing, the cylindrical samples were vacuum saturation using a BSJ fully automated saturator. The magnetic field conditions during the tests were set at 0.5 ± 0.05 T and a frequency of 21.3 Hz.

2.3.6. Compressive strength

Cubic samples with the size of 50 mm × 50 mm × 50 mm were prepared to assess the compressive strength of CT pastes. The samples were removed from the molds after hardening for one day, then cured to the corresponding age in a standard curing room at a temperature of 23±1 ℃ and relative humidity of over 95% according to ASTMC192 (36). The compressive strength testing of CT pastes was performed using a DYE-300 testing machine at a loading rate of 0.5 kN/s. The recorded compressive strength values were based on triplicate sample test averages.

2.3.7. Microstructure

A FlexSEM1000 scanning electron microscope was applied to investigate the influence of TCT on the microscopic properties of the pastes. Collecting specimens from 28d pastes and soaking in isopropanol alcohol for at least 7d to stop hydration, then vacuum drying for 24h. Before the test, the specimens were subjected to a 120 s gold-spraying procedure to enhance conductivity. The examination mode was SE with an accelerating voltage of 10 KV.

3. RESULTS AND DISCUSSIONS

3.1. Changes in the particle size and crystalline composition of CT due to thermal activation

3.1.1. XRD patterns of CT

Figure 2 shows the XRD patterns of CT. It reveals that all CT samples share a very similar composition with quartz, calcite, mayenite, lime, and gismondine as the major minerals. It can be seen that samples of Raw CT or calcined less than 700 °C displayed a sharp and obvious calcite peak at 2θ=29.4°, indicating an amount of high crystallinity calcite in CT. This calcite was used as filler in CT applications and does not participate in cement hydration. When calcined CT at 700 °C and above, this calcite peak gradually decreased sharply and even disappeared at 900°C, while the lime peak increased. This is related to the decomposition of $CaCO_3$ (700 °C—900 °C) (37) and produces highly reactive lime, which could contribute to enhancing the reactivity of CT.

3.1.2. Particle size

Figure 3 presents the particle size distributions of CT. It was found that the particle sizes ranges 300 μm to 400 μm of CT disappeared after thermal activation, as the curves TCT were shifted left, indicating that the thermal treatment has refined the size of CT. This is related to some CT particles expanding and causing fragmentation of particles, due to the calcination process. Furthermore, the refinement of CT particles became more prominent with the increased temperatures. For instance, a hump at about 30 μm emerges in the curve of TCT calcined at 700 ℃ and was gradually refined to less than 10μm as the calcined temperatures increased to 900 ℃. These refinements can be explained as the decomposed $CaCO_3$ within CT, resulting in a further break of CT particles. Meanwhile, the decomposition of $CaCO_3$ also produced highly active lime as shown in Figure 2, which may be conducive to enhancing the reactivity of CT.

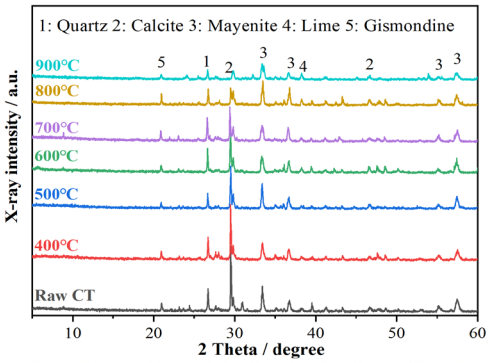

Quartz: SiO_2; Calcite: $CaCO_3$; Mayenite: $Ca_{12}Al_{14}O_{33}$; Lime: CaO; Gismondine: $Ca_2Al_4Si_4O_{16}{\cdot}9(H_2O)$

Figure 2. XRD patterns of CT.

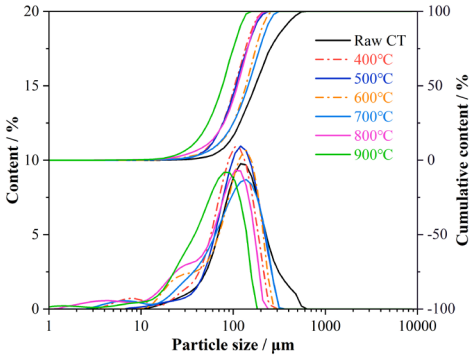

Note: Raw CT: untreated CT; X °C: CT thermally activated at X °C (X=400, 500, 600, 700, 800 or 900).

Figure 3. Particle size distributions of CT.

3.2. Setting time and fluidity of fresh mixtures

The addition of TCT has led to a significant acceleration in the setting process of cement, with the setting times reduced by 3%—10% (initial time) and 3%—16% (final time) relative to CT0, which is closely related to the activation temperature of TCT. A higher activation temperature, and a shorter setting time. This could be induced by the changes in both the chemical and physical properties of TCT. The calcination process of CT may induce the generation of more cracks in CT particles, which could absorb some mixed water, leading to less availability of free water during the mixing process. Meanwhile, the $CaCO_3$ in CT decomposed during 700 °C—900 °C and generated highly reactive lime, which can react rapidly with water for hydration resulting in shorter setting times (38, 39).

As can be seen from this table, the results of the fluidity of pastes also show a decreasing trend with the TCT subjected to elevated calcination temperature. By adding TCT calcine by 400 °C—900 °C, the reductions in the fluidity of pastes reach 6.0%—9.5% compared with CT0. Therefore, the changes in TCT due to the included cracks and increased lime content by high temperatures also influenced the fluidity of pastes, since less free water in mixtures to lubricate particles.

Table 3. Setting time and fluidity of CT pastes.

Mixtures	Initial time/min	Final time/min	Fluidity/cm
CT0	378	528	28.5
TCT4	365	505	26.8
TCT5	365	499	26.5
TCT6	360	495	26.5
TCT7	355	465	26.3
TCT8	340	453	26.3
TCT9	339	444	25.8

3.3. Hydration products

3.3.1. XRD analysis of the pastes

The XRD patterns of CT pastes at 3d and 28d are presented in Figure 4. The mineral phases identified in the samples include ettringite, quartz, calcite, $Ca(OH)_2$, C_3S, and C_2S, based on reference data and JCPDS files (40, 41). As shown in Figure 4a, the addition of TCT significantly intensified the peaks corresponding to $Ca(OH)_2$ at $2\theta = 18.0°$ and 34.2°. A higher calcination temperature of TCT resulted in even stronger peak intensities, indicating the production of more $Ca(OH)_2$. This is likely due to the decomposition of $CaCO_3$ in TCT, which generates lime that rapidly hydrates to form $Ca(OH)_2$ in the hydrating system. Additionally, the calcite peak at $2\theta = 29.4°$ was present in all samples, likely due to residual undecomposed $CaCO_3$ in the CT. Furthermore, some of the $Ca(OH)_2$ may have experienced carbonation during curing, contributing to the observed calcite in TCT8 and TCT9 samples. As the curing age was extended to 28d, the mineral compositions of the samples experienced very tiny changes as the patterns are similar to those of samples at 3d, as shown in Figure 4b. The intensity peak of $Ca(OH)_2$ of the pastes also displays an enhancing trend with the calcining temperature.

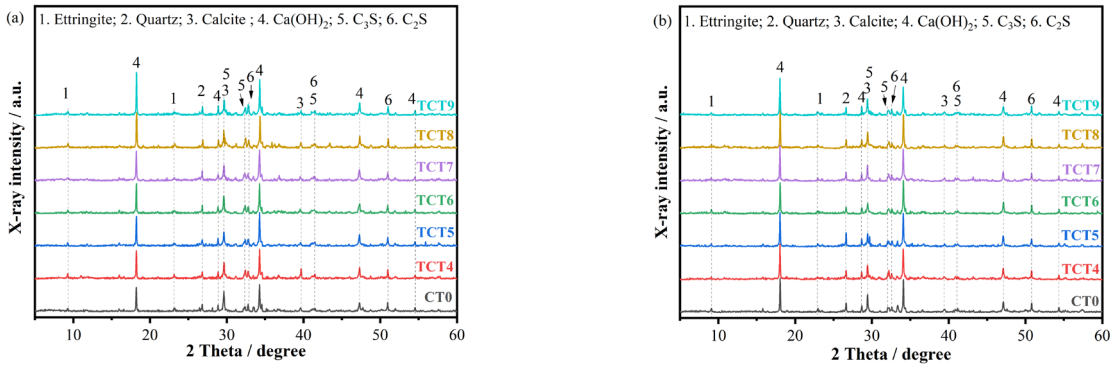

FIGURE 4. XRD patterns of CT pastes at 3d (a) and 28d (b).

3.3.2. TG-DTG analysis

Figure 5 presents the TGA results of CT pastes. Four obviously endothermic peaks were identified in the DTG curves corresponding to the decompositions of C-S-H and ettringite (80—105 °C), AFm (180—200 °C), $Ca(OH)_2$ (CH) (400—500 °C) and $CaCO_3$ (650—800 °C), respectively (42). The total mass loss of the pastes is closely related to the addition of TCT with different calcined temperatures, and a higher calcination temperature in TCT induced a higher mass loss for the pastes. This implies the increased decomposable substances in the TCT pastes as the increased peak of C-S-H, ettringite, and $Ca(OH)_2$, as revealed in the DTG curves. Figure 5c further clarified this observation, which increases by 0.34%—5.6% in C-S-H and ettringite, and 1.2%—6.8% in AFm. However, the increment in CH from TGA analysis would be lower with the real values, as some CH could be carbonated and produce $CaCO_3$, but also increasing by 0.9%—15.7% compared with CT0. Therefore, the TCT9 sample also shows a decomposition peak of $CaCO_3$, due to the carbonation of CH. Besides, this $CaCO_3$ peak in other samples may result from the undecomposed $CaCO_3$ in CT revealed by Figure 2 and some carbonated CH. The curved profiles of the mixtures at 28d are very similar to that of 3d. For instance, with the addition of TCT, the 28d pastes experience more mass loss during the heating process compared with CT0, as shown in Figures 5b and 5d. Nevertheless, the presence of C-S-H and ettringite in 28d samples was less than that of 3d, due to the carbonation of C-S-H and the transformation of ettringite into monocarboaluminate thus decreasing the content of these two hydration products (43).

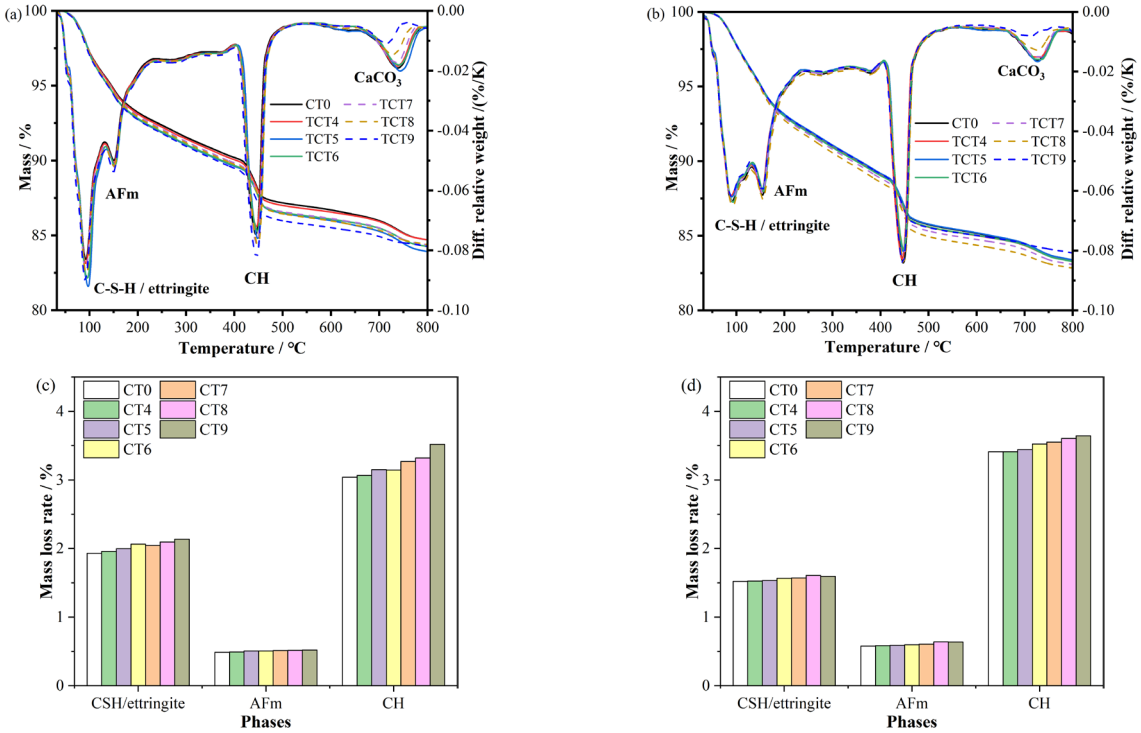

FIGURE 5. The results of TGA: (a) TG-DTG curves of CT pastes at 3d; (b) TG-DTG curves of CT pastes at 28d; (c) Mass loss rate of hydration products at 3d; (d) Mass loss rate of hydration products at 28d.

3.4. Pore size distribution

Figure 6 shows the pore structure of the 28d CT paste. The pore size distribution of the pastes shows a dual-peaked structure with the peaks located at 20 nm and 0.6 μm, representing capillary pores and air voids, respectively. The former is derived from the initial water-filled space not occupied by the hydrate (44), while the latter is result from incomplete compactness and residual air. It can be seen that the volumes of the air pores are decreased with the addition of TCT, which implies the refinement of the pore structure in CT pastes. This may be related to the acceleration effects of TCT during the setting process as revealed in Table 3, which reduces the contact of pastes and air. The addition of TCT also improves the capillary pores as the TCT4 peak in the curves decreases. Meanwhile, with increasing calcination temperature, the first peak of the pastes shifted left to 10 nm, suggesting that the TCT refined the pore size distribution of the pastes and reduced its porosity. This is possibly related to the refined sizes of CT particles by calcining, which could be filled in small pores. In addition, the volumes of these smaller pores obviously decreased when the CT calcined over 700 °C as the curves of TCT7—9 dropped off. This is consistent with the previous discussion. The reactive lime dissolves and releases additional Ca^{2+} into the system, while its hydration produces $Ca(OH)_2$, leading to an increased yield of hydration products. This promotes the formation and precipitation of more hydration products, contributing to the refinement of the pore structure within the paste.

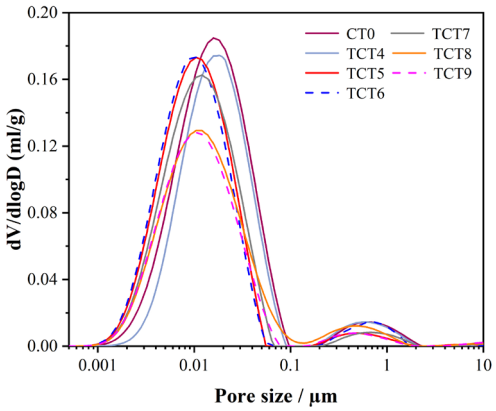

Figure 6. Pore size distribution of 28d CT pastes.

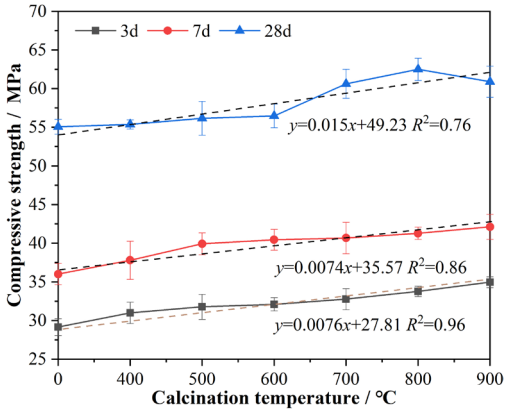

Figure 7. Compressive strength of CT pastes at 3d, 7d, and 28d.

3.5. Compressive strength

Figure 7 shows the compressive strength of CT pastes. It can be seen that the compressive strengths of the pastes increase gradually with the added TCT that calcined at higher temperatures. The linear-regression analysis shows that the 3d and 7d compressive strength are highly correlative with the calcination temperature, as can be expressed by Equations. [1] and [2].

$$y_{3d}=0.076x+27.81\ R^2=0.96 \quad [1]$$

$$y_{7d}=0.0074x+35.57\ R^2=0.86 \quad [2]$$

$$y_{28d}=0.015x+49.23\ R^2=0.76 \quad [3]$$

where x and y respectively represent the calcination temperature of CT and the compressive strength of samples at 3d or 7d. These two equations indicate that by adding calcined CT, the 3d and 7d compressive strengths of samples can be respectively improved by 6.8%—20.6% and 5%—16.9% based on CT0. This highlights the effects of calcination temperature in influencing the development of compressive strength of the pastes. The reason for this considerable increment in compressive strength is the finer CT particles result from the calcination process, resulting in a high surface area and density improving the internal structure of the pastes and increasing the density of the pastes. Additionally, highly active CaO was also produced by the decomposition of $CaCO_3$ in the calcination process, which can rapidly react with water in the pastes and promote the generation of hydration products shown in Figure 5c. At 28d, the compressive strength of pastes added TCT also increased according to CT0, increasing by 1.2%—13.5%. The results indicate that the compressive strengths of TCT9 are highest for 3d and 7d in all samples, but it is lower than that of TCT8 at 28d. This may be due to a rapid reaction of the TCT9 sample during the early age and promote the generation of hydration products, as the finer CT particles and more CaO produced in CT calcined at 900°C. This is similar to the findings of Rıza et al. on the compressive strength of cement mortar incorporating nano-CaO (45). They reported that a higher content of CaO in cement paste would result in a lower compressive strength at long curing ages. One possible reason for the reduction of compressive strength in TCT9 samples is that a higher CaO resulted in the formation of more $Ca(OH)_2$ in cement pastes shown in Figure 5d, which could induce expansion in the cement paste, thus decreasing the compressive strength.

3.6. Microstructure observation by SEM

Figure 8 presents the SEM images of CT pastes at 28d. The paste with raw CT shows a relatively loose and porous microstructure, characterized by voids and the presence of acicular AFt formations, indicating an incomplete filling of the matrix. In contrast, the paste containing CT calcined at 400 °C displays a slightly denser microstructure, although it still retains voids and hydration products, as shown in Figure 8b. The similarities to the CT0 sample suggest that these voids may limit densification and strength development of the pastes, as indicated in Figs 6 and 7. Figures 8c and 8d show the microstructure of the pastes with TCT calcined at temperatures of 800 °C and 900 °C. The $Ca(OH)_2$ crystals are well-defined and occupy some of the spaces within the structure, while the C-S-H gel appears as a more amorphous phase, contributing to the strength and binding of the matrix. This was consistent with the results of the TGA analysis. The addition of TCT introduces active CaO into the cement system, which can provide additional Ca^{2+} for the generation of Ca-containing products and accelerate cement hydration. Furthermore, as shown in Figure 3, the CT particles calcined at 800 °C and 900 °C have smaller particle sizes, which implies that finer pores within the paste can be filled, thereby enhancing the integrity of the matrix. However, a high CaO content might adversely affect the long-term strength of mortar, as reported by Rıza et al. (45). The $Ca(OH)_2$ generated from the hydration of CaO could induce expansion in the pastes, potentially reducing long-term compressive strength, as illustrated in Figure 7.

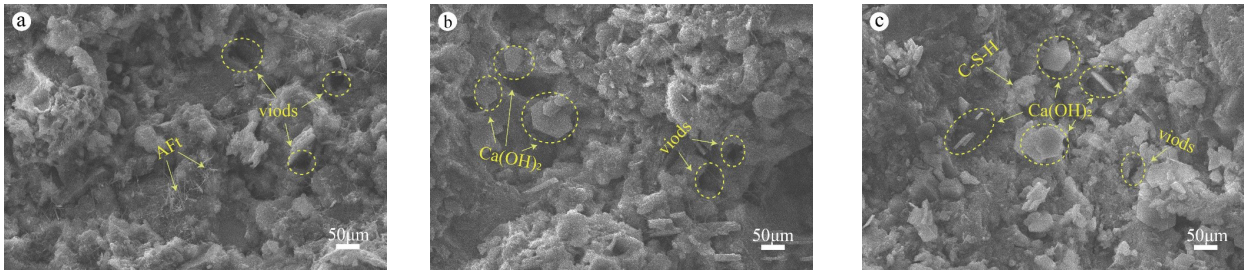

Figure 8. SEM images of CT paste at 28d: (a) CT0; (b) TCT4; (c) TCT8; (d)TCT9.

4. MECHANISM SUMMARY

The above results demonstrated that TCT can serve effectively as a supplementary cementitious material in a cement system without compromising compressive strength. Furthermore, the 3d and 7d compressive strength of the produced pastes can be respectively improved by 6.8%—20.6% and 5%—16.9% with the additions of TCTs subjected to 400 °C—900 °C, owing to both chemical and physical modifications for CT. By thermal treatment, the size of CT was reduced, and reactive CaO was produced in CT, where a higher calcination temperature for CT generally resulted in finer CT particles with more CaO. Therefore, the roles of the two changes in CT can be summarized. Firstly, the produced CaO in TCT accelerated the hydration of cement with the generation of more hydration products (i.e., C-S-H, $Ca(OH)_2$, and AFm) by offering additional Ca^{2+}. The hydration of the CaO also increases the amount of $Ca(OH)_2$ in the microstructure of the paste. Secondly, the smaller TCT particles along with the increased hydration products and the additional $Ca(OH)_2$ associated with CaO hydration refined the pore structure of the produced pastes with smaller porosities, contributing to the enhanced compressive strength.

Therefore, one can find that proper thermal treatment for CT can be an effective approach to converting CT into reactive TCT. In such a way, a promising disposal and utilization way for CT, which has very fine sizes and low recycling rates, can be established. This would benefit the world by providing a sustainable solution to reducing cement utilization, promoting CT utilization, and ensuring the normal production of copper metal.

5. CONCLUSIONS

This paper investigated the use of thermal activation to improve the reactivity of copper tailings and the effect of using thermally activated CT as a supplementary cementitious material on the hydration process of cement pastes. Experimental results revealed the setting time of pastes incorporating activated CT was reduced by 3%—10% (initial setting time) and 3%—16% (final setting time). XRD and TGA analyses revealed an increased generation of $Ca(OH)_2$ during the early stages of hydration, accompanied by greater mass loss upon heating, indicating an improved hydration process. This improvement effect was found to correlate with calcination temperatures of CT. In particular, pastes with activated CT (400 °C—900 °C) exhibited a linear relationship between compressive strength and calcination temperature at early ages, with improvements ranging from 6.8%—20.6% at 3d and 5%—16.9% at 7d compared to

the paste with raw CT. Although this linear trend diminished over time, the 28d compressive strength of the activated CT pastes still showed an increase of 1.2%—13.5%. These findings highlight the potential of thermally activated CT to improve the hydration of cement-tailings mixtures, contributing to both tailings management and environmental protection efforts. Future research could focus on optimizing the activation process, for example, by exploring the use of catalysts to lower the required activation temperature.

Acknowledgements

This study was funded by the National Natural Science Foundation of China (52008003), Outstanding Youth Project of Natural Science Research in Universities of Anhui Province (23AH030043), National Key Research and Development Plan (2021YFB3401504).

Authorship contribution statement

L. Wang: Conceptualization, Data cleansing, Formal analysis, Research, Visualization, Write-up - original draft, Write-up - review & editing.

H. Fang: Formal analysis, Supervision, Methodology.

P. Chen: Conceptualization, Fund raising, Write-up - review & editing, Supervision.

Z. Zong: Formal analysis, Validation.

P. Qian: Formal analysis, Validation.

X. Wang: Formal analysis, Validation.

Declaration of competing interest

The authors of this article declare that they have no financial, professional or personal conflicts of in-terest that could have inappropriately influenced this work.

REFERENCES

1. Xiaolong Z, Shiyu Z, Hui L, Yingliang Z. 2021. Disposal of mine tailings via geopolymerization. J. Clean. Prod. 284:124756. https://doi.org/10.1016/j.jclepro.2020.124756
2. Ghazi AB, Jamshidi-Zanjani A, Nejati H. 2022. Utilization of copper mine tailings as a partial substitute for cement in concrete construction. Constr. Build. Mater. 317:125921. https://doi.org/10.1016/j.conbuildmat.2021.125921
3. Maruthupandian S, Chaliasou A, Kanellopoulos A. 2021. Recycling mine tailings as precursors for cementitious binders–Methods, challenges and future outlook. Constr. Build. Mater. 312:125333. https://doi.org/10.1016/j.conbuildmat.2021.125333
4. Akinyemi BA, Alaba PA, Rashedi A, 2022. Selected performance of alkali-activated mine tailings as cementitious composites: A review. J. Build. Eng. 50:104154. https://doi.org/10.1016/j.jobe.2022.104154
5. Chen Q, Tao Y, Feng Y, Zhang Q, Liu Y. 2021. Utilization of modified copper slag activated by Na_2SO_4 and CaO for unclassified lead/zinc mine tailings based cemented paste backfill. J. Environ. Manage. 290:112608. https://doi.org/10.1016/j.jenvman.2021.112608
6. Vignesh R, Abdul-Rahim A. 2023. New insights into the production of sustainable synthetic aggregates and their microstructural evaluation. Mater. Construcc. 73(351):e324. https://doi.org/10.3989/mc.2023.328722
7. Lu K, Sun W, Gao T, Li Z, Zhao J, Cheng H. 2023. Preparation of new copper smelting slag-based mine backfill material and investigation of its mechanical properties. Constr. Build. Mater. 382:131228. https://doi.org/10.1016/j.conbuildmat.2023.131228
8. Gu J, Liu X, Zhang Z. 2023. Road base materials prepared by multi-industrial solid wastes in China: A review. Constr. Build. Mater. 373:130860. https://doi.org/10.1016/j.conbuildmat.2023.130860
9. Zhu K, He Y, Feng D, Jiang W, Zhang K. 2023. Leaching behavior of copper tailings solidified/stabilized using hydantoin epoxy resin and red clay. J. Environ. Manage. 345:118876. https://doi.org/10.1016/j.jenvman.2023.118876
10. Liu S, Li Q, Song J. 2018. Study on the grinding kinetics of copper tailing powder. Powder Technol. 330:105-113. https://doi.org/10.1016/j.powtec.2018.02.025
11. Jian S, Gao W, Lv Y, Tan H, Li X, Li B, Huang W. 2020. Potential utilization of copper tailings in the preparation of low heat cement clinker. Constr. Build. Mater. 252:119130. https://doi.org/10.1016/j.conbuildmat.2020.119130
12. Saedi A, Jamshidi-Zanjani A, Darban AK. 2020. A review on different methods of activating tailings to improve their cementitious property as cemented paste and reusability. J. Environ. Manage. 270:110881. https://doi.org/10.1016/j.jenvman.2020.110881
13. De Magalhaes LF, França S, Dos Santos Oliveira M, Peixoto RAF, Bessa SAL, Da Silva Bezerra AC. 2020. Iron ore tailings as a supplementary cementitious material in the production of pigmented cements. J. Clean. Prod. 274:123260. https://doi.org/10.1016/j.jclepro.2020.123260
14. Liu B, Xie Y, Zhou S, Yuan Q. 2000. Influence of ultrafine fly ash composite on the fluidity and compressive strength of concrete. Cem. Concr. Res. 30(9):1489-1493. https://doi.org/10.1016/S0008-8846(00)00323-9

15. Bonczyk M, Rubin J. 2022. The application of coal mining waste to the production of construction ceramics: radiological and mechanical aspects. Mater. Construcc. 72(348):e300. https://doi.org/10.3989/mc.2022.01822
16. Ghazi AB, Jamshidi-Zanjani A, Nejati H. 2022. Clinkerisation of copper tailings to replace Portland cement in concrete construction. J. Build. Eng. 51:104275. https://doi.org/10.1016/j.jobe.2022.104275
17. Wang Y, Zhao C, Chen P, Wang C, Tan W, Qian X, Qiao X. 2023. Preparation of mortars using bio-functionalized copper tailings. J. Build. Eng. 77:107460. https://doi.org/10.1016/j.jobe.2023.107460
18. Thomas BS, Damare A, Gupta R. 2013. Strength and durability characteristics of copper tailing concrete. Constr. Build. Mater. 48:894-900. https://doi.org/10.1016/j.conbuildmat.2013.07.075
19. Meena A, Singh N, Singh S. 2024. Shear strength and microstructural investigation on high-volume fly ash self-compacting concrete containing recycled concrete aggregates and coal bottom ash. Mater. Construcc. 74(353):e333. https://doi.org/10.3989/mc.2024.354623
20. Huang XY, Ni W, Cui WH, Wang ZJ, Zhu LP. 2012. Preparation of autoclaved aerated concrete using copper tailings and blast furnace slag. Constr. Build. Mater. 27(1):1-5. https://doi.org/10.1016/j.conbuildmat.2011.08.034
21. Moura WA, Gonçalves JP, Lima MBL. 2007. Copper slag waste as a supplementary cementing material to concrete. J. Mater. Sci. 42:2226-2230. https://doi.org/10.1007/s10853-006-0997-4
22. Onuaguluchi O, Eren Ö. 2012. Recycling of copper tailings as an additive in cement mortars. Constr. Build. Mater. 37:723-727. https://doi.org/10.1016/j.conbuildmat.2012.08.009
23. Jhatial AA, Nováková I, Gjerløw E. 2023. A review on emerging cementitious materials, reactivity evaluation and treatment methods. Buildings. 13(2):526. https://doi.org/10.3390/buildings13020526
24. Simonsen AMT, Solismaa S, Hansen HK, Jensen PE. 2020. Evaluation of mine tailings' potential as supplementary cementitious materials based on chemical, mineralogical and physical characteristics. Waste Manage. 102:710-721. https://doi.org/10.1016/j.wasman.2019.11.037
25. Kiventerä J, Piekkari K, Isteri V, Ohenoja K, Tanskanen P, Illikainen M. 2019. Solidification/stabilization of gold mine tailings using calcium sulfoaluminate-belite cement. J. Clean. Prod. 239:118008. https://doi.org/10.1016/j.jclepro.2019.118008
26. Zhang N, Tang B, Liu X. 2021. Cementitious activity of iron ore tailing and its utilization in cementitious materials, bricks and concrete. Constr. Build. Mater. 288:123022. https://doi.org/10.1016/j.conbuildmat.2021.123022
27. Singh V, Dixit P, Venugopal R, Venkatesh KB. 2019. Ore pretreatment methods for grinding: Journey and prospects. Miner. Process. Extr. Metall. Rev. 40(1):1-15. https://doi.org/10.1080/08827508.2018.1479697
28. Kiventerä J, Perumal P, Yliniemi J, Illikainen M. 2020. Mine tailings as a raw material in alkali activation: A review. Int. J. Miner. Metall. Mater. 27:1009-1020. https://doi.org/10.1007/s12613-020-2129-6
29. Zhao J, Zhang X, Sheng J, Wang Y, He G, Liu Q. 2023 Utilization of Coal gasification fine ash for construction material: From physical and chemical properties to the hydration activity of thermally modified CGFA. J. Environ. Chem. Eng. 11(6):111137. https://doi.org/10.1016/j.jece.2023.111137
30. Liebig E, Althaus E. 1998. Pozzolanic activity of volcanic tuff and suevite: effects of calcination. Cem. Concr. Res. 28(4):567-575. https://doi.org/10.1016/S0008-8846(98)00024-6
31. Fernandez R, Martirena F, Scrivener KL. 2011. The origin of the pozzolanic activity of calcined clay minerals: A comparison between kaolinite, illite and montmorillonite. Cem. Concr. Res. 41(1):113-122. https://doi.org/10.1016/j.cemconres.2010.09.013
32. Xiao L, Pang B. 2017. Experimental study on the effect of calcination on the volcanic ash activity of diatomite. IOP Conf. Ser. Mater. Sci. Eng. 231:012089. https://doi.org/10.1088/1757-899X/231/1/012089
33. Baki VA, Ke X, Heath A, Calabria-Holley J, Terzi C. 2024. Improving the pozzolanic reactivity of clay, marl and obsidian through mechanochemical or thermal activation, Mater Struct 57:9. https://doi.org/10.1617/s11527-023-02280-z
34. ASTM C191-21. 2021. Standard test methods for time of setting of hydraulic cement by Vicat needle. ASTM International.
35. ASTM C1437. 2020. Standard test method for flow of hydraulic cement mortar. ASTM International. https://doi.org/10.1520/C0143_C0143M-20
36. ASTM C192/C192M-19. 2020. Standard practice for making and curing concrete test specimens in the laboratory. ASTM International. https://doi.org/10.1520/C0192_C0192M-19
37. Sasaki K, Qiu X, Hosomomi Y, Moriyama S, Hirajima T. 2013. Effect of natural dolomite calcination temperature on sorption of borate onto calcined products. Microporous Mesoporous Mater. 171:1-8. https://doi.org/10.1016/j.micromeso.2012.12.029
38. Lee SE, Choi YC. 2024. Evaluating the potential of high free-CaO fluidized bed boiler ash as a cement admixture. Constr. Build. Mater. 439:137273. https://doi.org/10.1016/j.conbuildmat.2024.137273
39. Kang YH, Choi YC. 2018. Development of non-sintered zero-OPC binders using circulating fluidized bed combustion ash. Constr. Build. Mater. 178:562-573. https://doi.org/10.1016/j.conbuildmat.2018.05.184
40. Chernyavsky V, Kim A, Koshtyal Y, Rumyantsev A, Popovich A, Maximov MY. 2022. Structural features of complete and partial activation of Li-rich cathodes studied by in-situ XRD, Electrochim. Acta 414:140237. https://doi.org/10.1016/j.electacta.2022.140237
41. Pei C, Chen P, Tan W, Zhou T, Li J. 2023. Effect of wet copper tailings on the performance of high-performance concrete. J. Build. Eng. 74:106931. https://doi.org/10.1016/j.jobe.2023.106931
42. Knapen E, Van Gemert D. 2009. Cement hydration and microstructure formation in the presence of water-soluble polymers. Cem. Concr. Res. 39(1):6-13. https://doi.org/10.1016/j.cemconres.2008.10.003

43. Ipavec A, Gabrovšek R, Vuk T, Kaučič V, Maček J,Meden A. 2011. Carboaluminate phases formation during the hydration of calcite-containing Portland cement. J. Am. Ceram. Soc. 94(4):1238-1242. https://doi.org/10.1111/j.1551-2916.2010.04201.x
44. Ran B, Omikrine-Metalssi O, Fen-Chong T, Dangla P, Li K. 2023. Pore crystallization and expansion of cement pastes in sulfate solutions with and without chlorides. Cem. Concr. Res. 166:107099. https://doi.org/10.1016/j.cemconres.2023.107099
45. Polat R, Demirboğa R, Karagöl F. 2019. Mechanical and physical behavior of cement paste and mortar incorporating nano-CaO, Struct. Concr. 20(1):361-370. https://doi.org/10.1002/suco.201800132